Direct In Situ Measurement of Alkalinity Export

for Real-Time Enhanced Weathering MRV

Andrew Muth, Jonte Boysen, and Pascal Michel*

Everest Carbon, Berlin, Germany

E-mail: pascal@everestcarbon.com

Abstract

Accurate quantification of alkalinity export from the near-field zone remains a key

bottleneck for monitoring, reporting, and verification (MRV) of carbon dioxide removal

(CDR) through Enhanced Weathering (EW). Here we validate the Everest Pulsar,

a field-deployable alkalinity sensor that accumulates total alkalinity (TA) using a

weak acid ion-exchange resin and transduces resin saturation into a digital, in situ

measurement. In a 7-day continuous-flow soil column experiment (10 no-soil, 5 soil

units), the sensor quantitatively retained incoming alkalinity, with capture efficien-

cies of 98.9% (SD=0.3%) without soil and > 97.7% (SD=0.2%) with soil. Combined

capture-and-recovery efficiencies were 98.8% (SD=4.1%) and at least 93.9% (SD=1.3%)

for no-soil and soil units respectively. Effluent alkalinity remained well below 2% across

all loading states, and mass-balance residuals averaged 0.1% (SD=4.3%) without soil

and 4.0% (SD=1.3%) with soil. The digital readout closely matched chemically recov-

ered TA with an average deviation of -0.3% (SD=6.0%). These results provide the first

quantitative validation of an in situ sensor capable of measuring cumulative alkalinity

export and demonstrate a practical path toward accurate, cost-effective, real-time MRV

of EW carbon removal.

1

Introduction

Enhanced weathering (EW) represents a promising geochemical pathway for durable carbon dioxide removal (CDR), leveraging abundant silicate rocks and existing technology for material sourcing, bulk transportation and farmland distribution to achieve gigaton-scale impacts within decades. Early projections estimated $2.0 - 4.0 \,GtCO_2 \,yr^{-1}$ potential globally^{1,2}, with a recent estimate showing $0.16 - 0.30 \,GtCO_2 \,yr^{-1}$ potential by mid-century in the US³. EW speeds up natural rock weathering by applying finely ground silicates (e.g., basalt or olivine) to soils, where carbonic acid dissolves the minerals, releasing base cations (Ca²⁺, Mg²⁺, K⁺, Na⁺) and producing bicarbonate (HCO₃⁻). This additional export of total alkalinity (TA) ultimately facilitates long-term CO_2 sequestration in groundwaters and oceans¹.

State-of-the-art monitoring, reporting, and verification (MRV) protocols for EW rely on solid-phase and aqueous-phase analyses to estimate CDR⁴⁻⁶. Solid-phase approaches target measurements of the cation mass balance in the soil column (e.g. TiCAT⁷). They intrinsically offer upper-bound estimates of potential CDR that are confounded by cation retention, secondary mineral formation, and time lags before alkalinity export from the near-field zone and thereby permanence of captured carbon is realized^{8,9}. Noisy backgrounds and field heterogeneity are known challenges⁶. In typical aqueous-phase methods alkalinity export is measured ex-situ in porewater samples. While providing direct evidence and a lower bound of dissolved weathering products^{10–12}, porewater sampling is known to suffer from logistical challenges, ¹³ discontinuous point-in-time measurements, which can skew results ^{14,15} and high labor demand⁵. These limitations hinder scalable and accurate quantification of alkalinity export and present the most critical bottleneck for ERW scale-up today.

Ion-exchange resins offer an alternative strategy by accumulating ions from percolating soil water for later analysis. Strong-acid and strong-base resins have been applied across diverse soil systems to estimate nutrient leaching and ion fluxes ^{16–20}. For EW applications, these

approaches face practical constraints: mixed-bed strong resins sorb nearly all mobile ions, leading to competitive site occupation in chemically complex soil matrices. Moreover, quantitative readout requires labor- and cost-intensive ICP-MS and IC analyses, including careful elution and matrix correction.

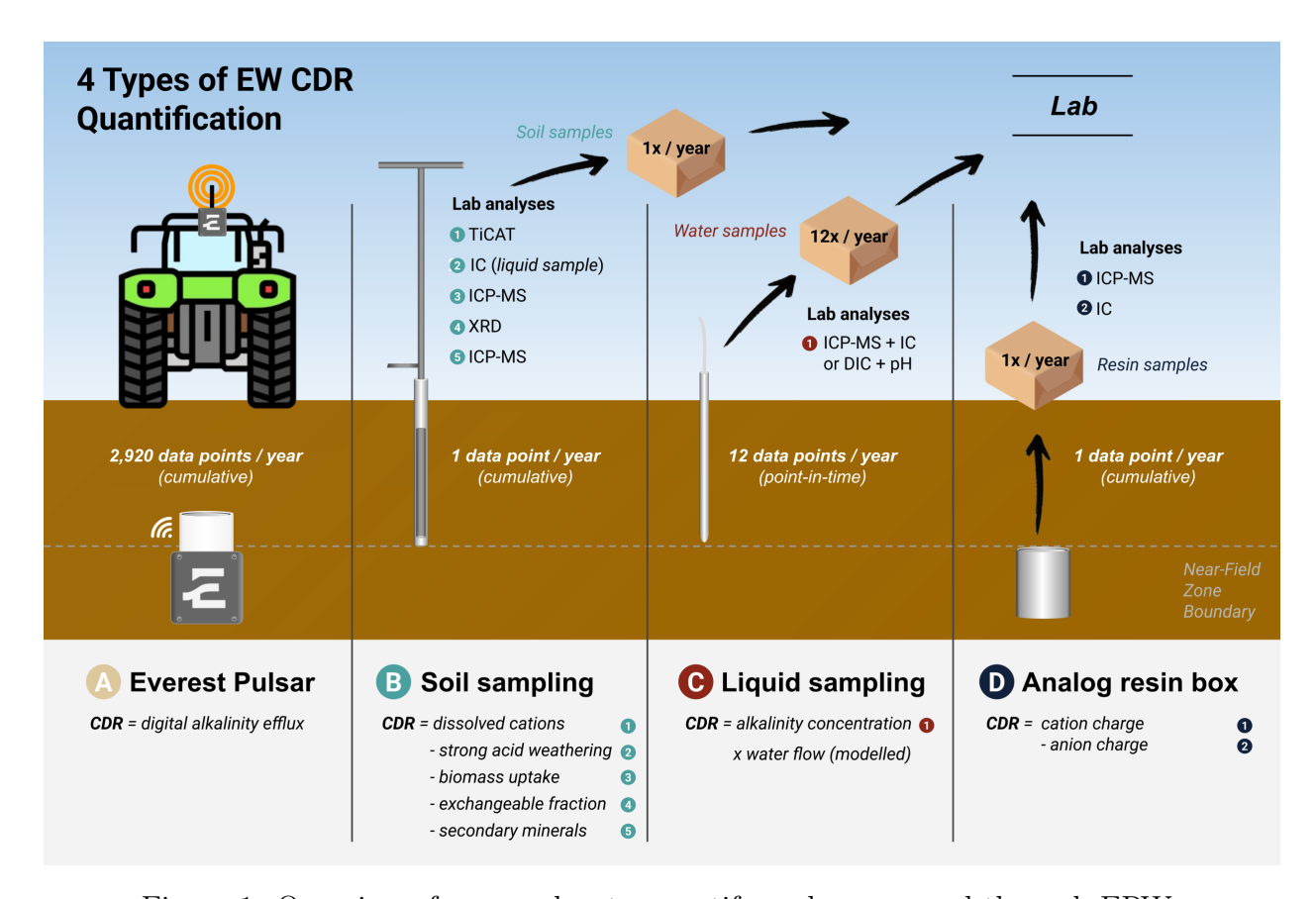


Figure 1: Overview of approaches to quantify carbon removal through ERW.

Here we validate the *Everest Pulsar*, a third-generation field-deployable alkalinity sensor designed specifically for EW MRV. The Pulsar uses weak acid resins*, whose higher- pK_a functional groups selectively capture cations contributing to total alkalinity while remaining unreactive toward neutral salts^{21,22}. This provides inherent correction for non-carbonic acid weathering and enables simple, accurate quantification of captured TA via acid-base titration. Further, Pulsar integrates a proprietary electronic readout that converts the resin

^{*}International Patent Pending

saturation state into a cumulative digital TA signal, which is uploaded for real-time remote monitoring*.

In this study, we provide the first quantitative validation of this approach. Using controlled soil-column experiments, we evaluate (i) the capture efficiency of weak-acid resins under usual deployment alkalinity loadings, (ii) the completeness and accuracy of chemical recovery, and (iii) the agreement between digital and chemically measured cumulative TA. These results establish evidence of the first platform capable of real-time, in situ measurement of cumulative alkalinity export and open a practical path toward scalable MRV of EW carbon removal.

Methods

Experimental Setup

To quantify alkalinity capture and digital sensor performance under controlled yet realistic soil percolation conditions, we constructed a pump-driven soil-column system consisting of 19 sensor units mounted vertically on a custom-built stand (Figure 2). Each unit received a prescribed input alkalinity flux generated by individual peristaltic pump channels operated at $2.0 \pm 0.1 \, mL \, min^{-1}$, corresponding to a percolation rate of $15.3 \, mm \, h^{-1}$ through the sensor cross-section ($A = 78.54 \, cm^2$). The flow rate was chosen to be consistent with typical percolation rates of loamy sand soils²³.

Ten sensors were operated without soil, five with a 10 cm soil column placed above the sensor's flow control, and four served as DI-water dummy sensors, which are used to calibrate the digital TA signal and compensate for environmental noise like temperature. Figure 8 in the appendix shows field data demonstrating the efficacy of this calibration approach. All alkalinity inputs were supplied as 4.2 mM sodium bicarbonate $(NaHCO_3)$, prepared

gravimetrically from analytical-grade reagent in DI-water. Flow rates for all channels were verified before the experiment by gravimetric calibration.

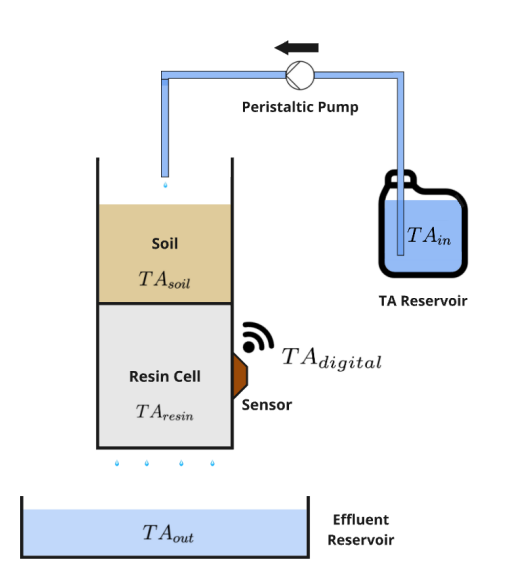




Figure 2: Schematic of the soil-column experiment showing the sensor-soil assembly, peristaltic pump system, and input/effluent reservoirs (left). Photograph of the 19-unit setup (10 no-soil, 5 soil, 4 dummy sensors) mounted on a custom-built rack (right). Flow was maintained at $2.0 \pm 0.1 \, mL \, min^{-1}$ per unit.

Soil Preparation and Characterization

Approximately 10 kg of soil was collected from an agricultural field north of Berlin, Germany. The material was air-dried, sieved (< 2 mm), homogenized, and two subsamples were submitted to an accredited external laboratory for determination of effective cation-exchange capacity (CEC) and base-saturation using the $BaCl_2$ extraction method in accordance with DIN ISO 11260:2018–11. Measured texture, cation-exchange capacity (CEC), and base saturation are summarized in Table 1.

Each soil-covered unit received $750 \pm 5\,g$ dry soil corresponding to a 10 cm layer height. Soil was pre-wetted with 600 mL DI water to minimize transient infiltration effects upon startup.

Table 1: Texture, effective CEC, and major cation concentrations of the soil before the experiment. Measurement uncertainty in cation concentrations was given as 30%.

Property	Sample 1	Sample 2	Mean
Sand (%)	84.4	84.6	84.5
Silt (%)	10.2	10.1	10.2
Clay $(\%)$	5.4	5.3	5.4
$Ca CEC (cmol kg^{-1})$	6.66	5.60	6.13
$Mg CEC (cmol kg^{-1})$	0.58	0.56	0.57
$K \text{ CEC (cmol kg}^{-1})$	0.42	0.46	0.44
Na CEC (cmol kg^{-1})	< 0.05	< 0.05	< 0.05
Base saturation (%)	76.6	73.2	74.9
Total CEC (cmol kg^{-1})	10.1	9.1	9.6

Analytical Measurements

Input Alkalinity (TA_{in})

For each 5 L $NaHCO_3$ reservoir, initial and final masses were recorded gravimetrically allowing volume delivery to be determined with <0.1% uncertainty. At constant concentration within each reservoir, cumulative input alkalinity was calculated as:

$$TA_{in}(t) = \int Q(t) c(t) dt = \sum_{i} (V_{\text{start},i} - V_{\text{end},i}) c_i$$
(1)

Gaussian error propagation resulted in <0.012 mmol alkalinity uncertainty per reservoir, corresponding to >99.9% accuracy of input alkalinity over the experiment.

Table 2: Overview of measurements used to constrain the system alkalinity cation mass balance.

Metric	Measurement	Error	Approach	Frequency
TA_{in}	Input TA ($tCO_2e ha^{-1}$)	$< \pm 0.001$	Gravimetric	Daily
TA_{soil}	Base cations (cmol kg^{-1})	$\pm 30\%$	DIN ISO 11260:2018–11	Start and endpoint
TA_{resin}	TA recovery $(tCO_2e ha^{-1})$	± 0.05	Extract resin and back-titrate	1–2 devices per day
TA_{out}	Effluent sodium $([Na^+])$	$\pm 0.5\%$	Ion Selective Electrode (ISE)	Daily

Soil-Retained Alkalinity (TA_{soil})

Post-experiment soil from each sensor was analyzed externally again using the $BaCl_2$ extraction method in accordance with DIN ISO 11260:2018–11. Soil-retained alkalinity per sensor was determined as the increase in exchangeable base-cation inventory $cat \in \{Ca^{2+}, Mg^{2+}, Na^+, K^+\}$ relative to the mean of the baseline sub-samples as

$$TA_{soil} = m_{soil} \Delta Q_{cat} = m_{soil} \left(\sum_{cat} q_{cat} [cat]_{soil,post} - \sum_{cat} q_{cat} [\bar{cat}]_{soil,pre} \right)$$
(2)

with q_{cat} representing the cation charge (2 for Ca^{2+} and Mg^{2+} , 1 for Na^+ and K^+).

Resin-Recovered Alkalinity (TA_{resin})

After extraction, the weak acid resin was transferred to Class-A glassware and eluted overnight with 100 mL of 0.5 M H_2SO_4 . Following three DI-water rinses, the combined eluates were titrated to pH 7.0 with 1 M NaOH using a calibrated Mettler Toledo InLab Expert Pro-ISM pH electrode (± 0.01 pH accuracy). Acid blanks and unused resin blanks were used to correct systematic offsets. Analytical uncertainty on titrated TA was $0.05 \ tCOe \ ha^{-1}$.

Effluent Alkalinity (TA_{out})

Effluent samples were collected daily in 50 mL HDPE vials. Sodium concentration was measured using a Mettler Toledo PerfectIONTM Na ISE calibrated with gravimetrically prepared NaCl standard solutions. The electrode range $(10^{-7}-1\,M)$ spans the required concentration window, though analytical variability increases below $\approx 1\%$ of input concentration. We therefore adopt an uncertainty of $\pm 0.5\%$ of the input amount for effluent measurements. Effluent alkalinity cation charge was calculated by

$$TA_{out} = \int_0^{V_{out}} [Na^+]_{out}(V) dV$$
 (3)

Mass-Balance Framework

At any point in time total alkalinity in the system must satisfy:

$$TA_{in} = TA_{soil} + TA_{resin} + TA_{out} + \zeta_{TA} \tag{4}$$

with ζ_{TA} being the mass balance closure error. All TA values are measured as cumulative molar cation charge and converted to $tCO_2e\ ha^{-1}$ based on the sensor cross-section.

Sensor Performance Metric

We evaluate Pulsar's performance along three key metrics that quantify (1) completeness of chemical adsorption of alkaline species, (2) completeness of chemical recovery through back-titration, and (3) deviation of the sensors digital TA signal from back-titrated TA.

1. Capture efficiency

$$\eta_{\text{capture}} = 1 - \frac{\text{TA}_{\text{out}}}{\text{TA}_{\text{in}} - \text{TA}_{\text{soil}}}$$
(5)

2. Capture-and-recovery efficiency

$$\eta_{\text{recovery}} = \frac{\text{TA}_{\text{resin}}}{\text{TA}_{\text{in}} - \text{TA}_{\text{soil}}} \tag{6}$$

3. Digital deviation

$$\Delta_{\text{digital}} = \frac{\text{TA}_{\text{digital}} - \text{TA}_{\text{resin}}}{\text{TA}_{\text{resin}}} \tag{7}$$

Results and Discussion

Soil Retention of Alkalinity

Post-experiment soil analyses revealed a significant (p < 0.001) increase in exchangeable Na⁺ and depletion of Ca²⁺, Mg²⁺, and K⁺ (Table 3). The fact that significantly more cation charge (ΔQ_{cat}) was released than monovalent Na⁺ charge retained rules out classical $Na^+ \leftrightarrow Ca^{2+}/Mg^{2+}$ exchange as the dominant process. Instead, desorption of native exchangeable cations induced by the low ionic strength of the dilute NaHCO₃ inflow, as well as the initial DI flush, seems the most likely explanation.

Table 3: Absolute change in exchangeable cations relative to pre-experiment (Table 1).

Property	Sensor 1	Sensor 2	Sensor 3	Sensor 4	Sensor 5
$TA_{in}(cmol(+) kg^{-1})$	6.43	6.28	5.00	4.67	8.38
$\Delta Q_{cat} \; (\text{cmol}(+) \; \text{kg}^{-1})$	-4.10	-5.16	-5.90	-4.88	-4.57
$\operatorname{Ca} \left(\operatorname{cmol}(+) \operatorname{kg}^{-1} \right)$	-4.14	-5.00	-5.72	-4.72	-4.5
$Mg (cmol(+) kg^{-1})$	-0.48	-0.58	-0.58	-0.52	-0.52
$K \text{ (cmol(+) kg}^{-1})$	-0.34	-0.34	-0.34	-0.32	-0.34
$Na (cmol(+) kg^{-1})$	0.86	0.76	0.74	0.68	0.79
Base saturation $(\%)$	-0.52	-2.66	-4.01	-1.10	-1.94
Total CEC (cmol kg^{-1})	-2.40	-2.99	-3.40	-2.98	-2.63

Under our root-free, respiration-limited conditions, desorbed divalent cations are exported primarily as neutral salts, contributing no additional alkalinity. Any true alkalinity-exporting cation exchange (e.g., $CaX_2 + 2NaHCO_3 \rightarrow 2NaX + Ca(HCO_3)_2$) would have been quantitatively captured given that weak acid resins have higher affinity for divalent cations than for monovalent cations due to their ability to bind to more than one charged functional group of the resin. ²² Consequently, we can give a conservative lower and upper bound for retained soil alkalinity (TA_{soil}), corresponding to zero (no alkalinity retained) and the observed increase in exchangeable Na⁺ (maximum potential fraction of input alkalinity retained), yielding the reported range in Table 4. The correlation between the upper range of TA_{soil} and input alkalinity TA_{in} is low (r = 0.59), underlining that the true expected retained alkalinity lies within the upper and lower bound.

Table 4: Retained total alkalinity TA_{soil} for each sensor given as range between its upper and lower bound.

Property	Sensor 1	Sensor 2	Sensor 3	Sensor 4	Sensor 5
$TA_{in} (tCO_2 ha^{-1})$	2.71	2.65	2.11	1.97	3.54
$TA_{soil} \text{ (tCO}_2 \text{ ha}^{-1}\text{)}$	[0, 0.36]	[0, 0.32]	[0, 0.31]	[0, 0.29]	[0, 0.33]

Capture Efficiency

Effluent sodium concentrations normalized to input concentrations are shown in Figure 3. Initial measurements on days 1-2 exhibited elevated and inconsistent values for several units due to transient contamination. For a weak-acid cation-exchange system receiving constant influent alkalinity and steady flow, effluent concentrations should increase smoothly with cumulative loading. Early effluent should be near zero while exchange sites are unsaturated, rising as capacity is approached. No physical or chemical mechanism under these conditions can produce an early spike. The elevated initial three sampling times therefore indicate contamination of the collection buckets rather than true breakthrough and were excluded from further analysis.

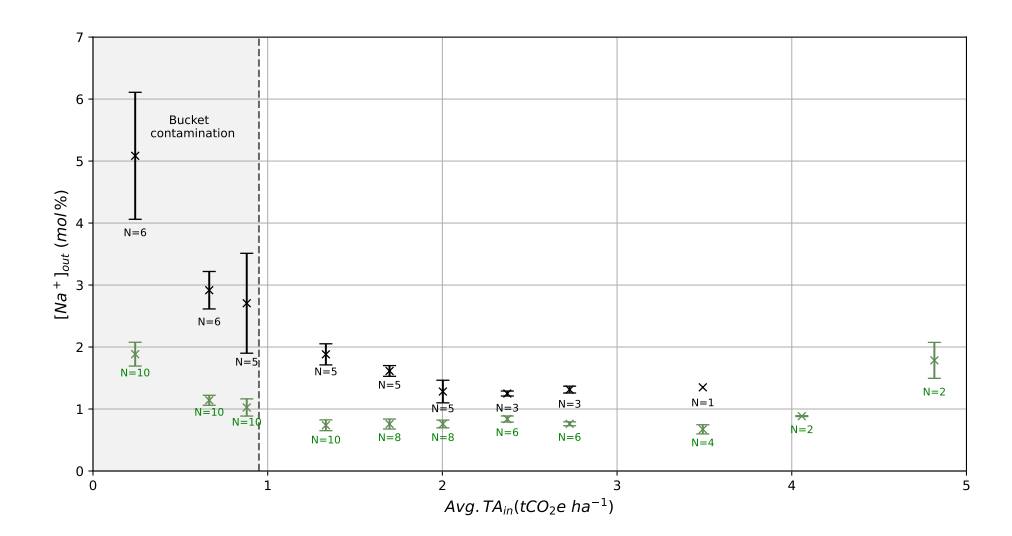


Figure 3: Effluent sodium concentrations $[Na^+]_{out}$ as a function of average applied alkalinity TA_{in} . Green points denote no-soil devices; black points denote soil devices. Error bars represent the standard deviation of measurements and N indicates the number of samples contributing at each collection time. The grey shaded region marks the samples excluded from analysis due to initial effluent collection bucket contamination.

Following this exclusion, effluent concentrations stabilized across all devices. Effluent alkalinity of no-soil units remained below 1.0% of input alkalinity until $\approx 4 \text{ tCO}_2 \text{ ha}^{-1}$ loading and increased modestly to $1.8 \pm 0.5\%$ at $\approx 5 \text{ tCO}_2 \text{ ha}^{-1}$, consistent with the onset of resin saturation. Effluent alkalinity of soil-covered devices remained below 2%, with higher apparent values attributable to ISE interference from soil colloids. Across all loading states, inter-sample standard deviations were < 0.25% and repeated ISE measurements showed intra-sample variations of up to 0.5% which we assume as accuracy and precision error of the effluent measurement respectively. Given the smoothness of effluent concentrations, we can simplify eq. (3) as:

$$TA_{out} = \frac{V_{out}}{n} \sum_{i=1}^{n} [Na^+]_{i,out}$$

$$\tag{8}$$

Propagating the range of retained alkalinity from Table 4, we find a mean capture efficiency of 97.7% (SD=0.2) to 97.9% (SD=0.2) for soil, and 98.9% (SD = 0.3%) for no-soil conditions.

Table 5: Calculated capture efficiencies. All values are reported in $tCO_2e\ ha^{-1}$ unless stated otherwise. Retained alkalinity TA_{soil} , and thus capture efficiency for soil units, is given as lower-upper bound range here.

Sensor	1	2	3	4	5
TA_{in}	2.71	2.65	2.11	1.97	3.54
TA_{soil}	[0, 0.36]	[0, 0.32]	[0, 0.31]	[0, 0.29]	[0, 0.33]
TA_{out}	0.06	0.05	0.04	0.04	0.08
$\eta_{capture}$	[97.5,97.8]%	[97.9,98.1]%	[97.8,98.1]%	[97.6,98.0]%	[97.5,97.7]%

Sensor	6	7	8	9	10	11	12	13	14	15
TA_{in}	1.96	2.12	2.62	1.30	3.52	1.28	3.55	2.55	5.22	5.11
TA_{soil}	-	-	-	-	-	-	-	-	-	-
TA_{out}	0.02	0.02	0.03	0.02	0.03	0.02	0.03	0.02	0.06	0.05
$\eta_{capture}$	99.0%	99.1%	98.9%	98.5%	99.1%	98.4%	99.2%	99.2%	98.9%	99.0%

As a conservative approach, we default to the pessimistic end of the retained alkalinity range (Table 5) for reported values, yielding 97.7% (SD=0.2) as the mean capture efficiency for soil columns and 98.5% (SD = 0.6%) as average capture efficiency across all devices. We conclude that capture of alkalinity is quantitative with effluent alkalinity remaining below

2% of input alkalinity across loading states and expected capture efficiency being at least 97.7% under soil conditions.

Capture-and-Recovery Efficiency

Propagating the range of retained alkalinity from Table 4, we find a mean capture and recovery efficiency of 93.9% (SD=1.3) to 107.6% (SD=2.6) for soil, and 98.8% (SD = 4.1%) for no-soil conditions. As before, we default to the pessimistic end of the retained soil alkalinity range and take 93.9% (SD=1.3) as the conservative lower bound of the mean capture and recovery efficiency for the soil-column devices. Sensor-level values are shown in (Table 6). Figure 4 shows back-titrated values TA_{resin} and measured effluent sodium concentrations across loading states, demonstrating close agreement of captured and recovered alkalinity to ground-truth and nine out of fifteen devices lying within a $\pm 5\%$ margin of the ideal 1:1 line. Deviations at high loading states remain small even as the resin saturates.

While the lower bound of the soil capture and recovery efficiency is non-quantitative, it has to be noted that the true expected efficiency is likely higher as discussed in the following section. In aggregate these results demonstrate that alkalinity capture and recovery in weak-acid resins via back-titration is efficient and most likely quantitative under soil percolation conditions.

Table 6: Comparing titrated alkalinity TA_{resin} versus alkalinity that entered the device $TA_{in} - TA_{soil}$. All values are reported in $tCO_{2}e\,ha^{-1}$ unless indicated otherwise. Mean capture-and-recovery efficiency is 98.8% (SD=4.1%) and at least 93.9% (SD=1.3%) for no-soil and soil devices respectively.

Sensor	1	2	3	4	5
$TA_{in} - TA_{soil}$	[2.35, 2.71]	[2.33, 2.65]	[1.80, 2.11]	[1.68, 1.97]	[3.20, 3.54]
TA_{resin}	2.57	2.49	2.02	1.81	3.31
$\eta_{recovery}$	[94.8, 109.3]%	[94.1, 107.0]%	[95.5, 111.9]%	[91.6, 107.4]%	[93.6, 103.3]%

Sensor	6	7	8	9	10	11	12	13	14	15
$TA_{in} - TA_{soil}$	1.96	2.12	2.62	1.30	3.52	1.28	3.55	2.55	5.22	5.11
TA_{resin}	1.98	2.13	2.55	1.36	3.38	1.37	3.31	2.49	5.01	4.86
$\eta_{recovery}$	101.0%	100.1%	97.5%	104.1%	96.0%	107.0%	93.3%	97.7%	95.9%	95.1%

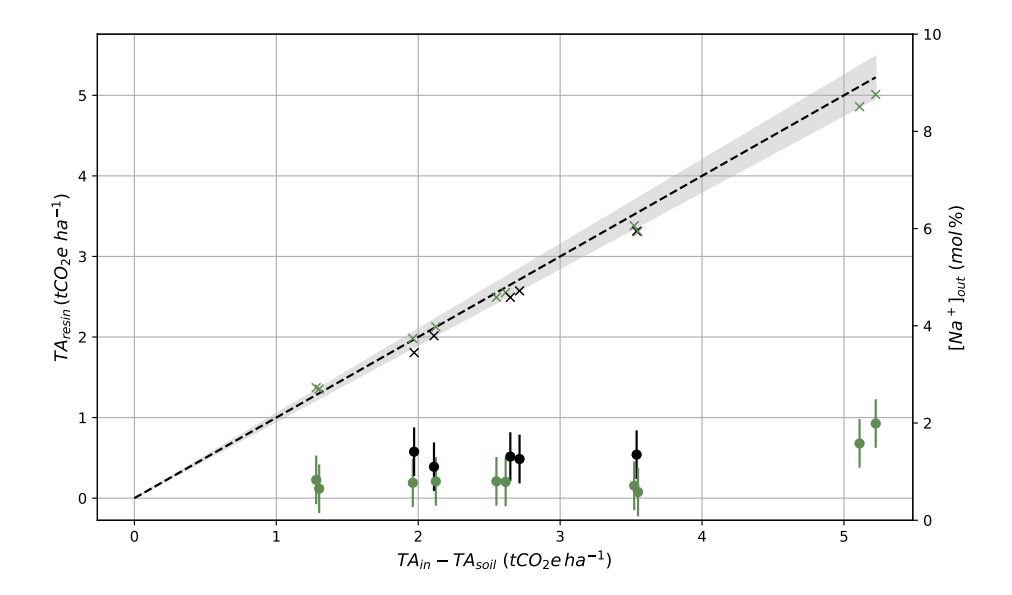


Figure 4: Back-titrated alkalinity TA_{resin} and effluent sodium concentrations $[Na^+]_{out}$ plotted against input alkalinity corrected for soil retention $(TA_{in} - TA_{soil})$. Green symbols denote no-soil devices and black symbols soil devices (crosses: titrations; circles: effluent measurements, with error bars indicating analytical uncertainty). The dashed line represents the 1:1 ideal relationship, and the shaded band indicates a $\pm 5\%$ margin. Titration results closely follow the ideal line across loading states, while effluent alkalinity remains low even at higher loadings.

Mass-Balance Closure

Full mass-balance closure was achieved with a very low mean residual alkalinity of 0.1% (SD=4.3) for sensors without soil, while mean residual alkalinity for sensors with soil remained 4.0% (SD=1.3) when adopting the conservative lower bound assumption of $TA_{soil} = 0$ (Table 7). In both cases, the residuals followed a Gaussian distribution (Shapiro-Wilk p=0.45, no-soil; Shapiro-Wilk p=0.34, soil) as visualized in Figure 5.

While both datasets exhibit comparable normally distributed measurement noise, the soil sensors display a systematic positive bias. The near-zero mean residual in the no-soil case, together with its $\approx 4\%$ standard deviation, agrees with the combined uncertainties from gravimetric dosing, ISE analysis, and titration, indicating that all TA-associated cation charge is quantitatively accounted for in the no-soil system.

Table 7: Per-device mass-balance closure. All quantities are normalised by and reported in percent of TA_{in} .

Sensor	1	2	3	4	5	6	7	8	9	10	11	12	13	14	15
TA_{in}	100	100	100	100	100	100	100	100	100	100	100	100	100	100	100
$-TA_{soil}$	0	0	0	0	0	-	-	-	-	-	-	-	-	-	-
$-TA_{resin}$	94.8	94.1	95.5	91.6	93.6	101.0	100.1	97.6	104.1	96.0	107.0	93.3	97.7	95.9	95.1
$-TA_{out}$	2.2	1.9	1.9	2.0	2.3	1.0	0.9	1.2	1.5	0.9	1.6	0.8	0.8	1.2	1.0
$=\zeta_{TA}$	2.9	4.0	2.7	6.3	4.1	-2.0	-1.0	-1.3	-5.6	3.2	-8.6	5.8	1.5	2.9	3.9

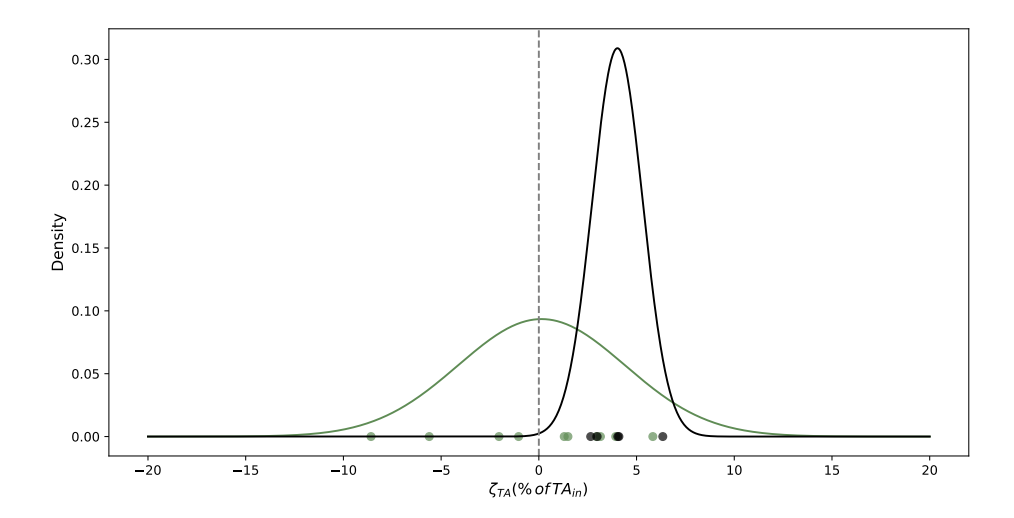


Figure 5: Residual alkalinity distributions for sensors with soil (black) and without soil (green). Points show individual mass-balance residuals, and curves show fitted Gaussian distributions. The mean and standard deviation of the no-soil residuals are 0.1~% and 4.3~% respectively, while soil residuals have mean and SD of 4.0~% and 1.3~% respectively.

A complementary way to interpret the residuals is by expressing capture efficiency as a function of capture-and-recovery efficiency (Eqs. 5, 6) via the alkalinity mass balance (Eq. 4):

$$\eta_{capture} = \eta_{recovery} + \frac{\zeta_{TA}}{TA_{in} - TA_{soil}} \tag{9}$$

Equation 9 clarifies why $\eta_{recovery} \approx \eta_{capture}$ (98.8% vs. 98.9%) for no-soil sensors where $\zeta_{TA} \approx 0$, whereas the soil sensors exhibit $\eta_{recovery} \approx \eta_{capture} - 4\% \, TA_{in}$ (>93.9% vs. >97.7%) because $\zeta_{TA} \approx 4\% \, TA_{in}$ under the assumption $TA_{soil} = 0$. Given the low analytical error of the ISE measurement and titration, as well as the higher affinity of weak-acid resin for divalent cations that contribute charge-equivalently to the titration, the observed residuals are unlikely to be fully explained by analytical uncertainty or a systematic error other than soil

related. Instead, the more consistent interpretation is that the residuals represent unmeasured alkalinity retained within the soil column, rather than sensor bias. Accordingly, and with appropriate caution, we conclude that the true expected capture-and-recovery efficiency under soil conditions is likely closer to the observed capture efficiency (97.7%), supporting quantitative capture and recovery of alkalinity in the integrated soil—sensor system.

Digital Sensor Performance

The Pulsar's digital TA signal $TA_{digital}$ closely tracked cumulative TA uptake in both soil and no-soil devices. A dummy sensor exposed to alternating DI water and TA solution exhibited the expected stable baseline and linear signal increase (Figure 4). Table 8 compares digital TA signal and captured and recovered alkalinity for all sensors. The mean digital deviation $\Delta_{digital}$ was -3.5% (SD=3.6%) for sensors without soil, 6.2% (SD=4.6%) for sensors with soil, and -0.3% (SD=6.0%) overall. The bias observed in both soil-covered and uncovered units falls within the distribution width of the cohort. The average consistency of digital outputs demonstrates that the electronic readout provides a robust in situ measurement of cumulative alkalinity uptake.

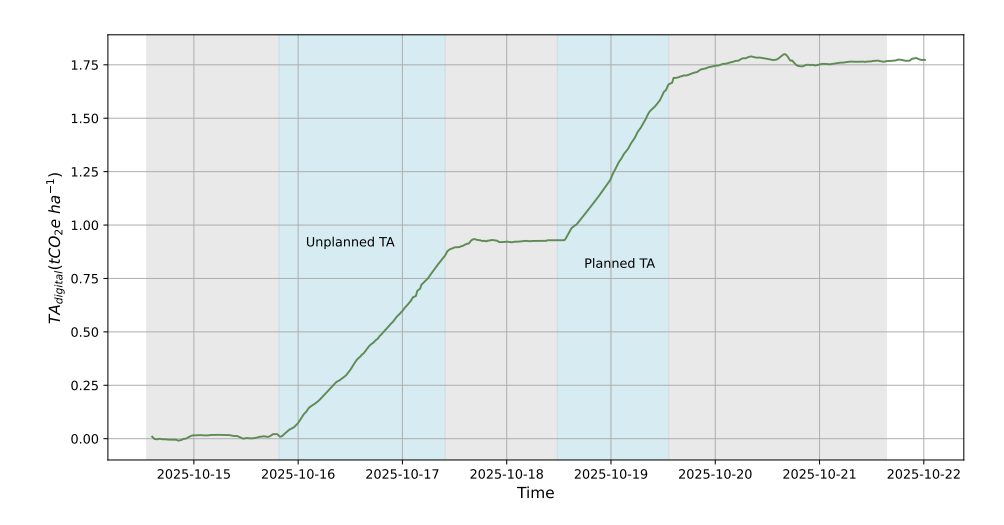


Figure 6: Digital signal from a dummy sensor alternately exposed to DI water and alkalinity solution, demonstrating stable baseline under neutral DI inflow (grey area) and linear signal increase during alkalinity influx (blue area).

Table 8: Digital TA measurements $TA_{digital}$ compared against captured and recovered alkalinity TA_{resin} and resulting deviations $\Delta_{digital}$. All values are reported in $tCO_2e\ ha^{-1}$ unless stated otherwise

Sensor	1	2	3	4	5	6	7	8	9	10	11	12	13	14	15
TA_{resin}	2.57	2.49	2.02	1.81	3.31	1.98	2.13	2.55	1.36	3.38	1.37	3.31	2.49	5.01	4.86
$TA_{digital}$	2.57	2.63	2.08	2.05	3.61	1.91	2.06	2.62	1.27	3.44	1.24	3.24	2.35	4.89	4.54
$\Delta_{digital}$	0.0%	5.7%	3.0%	13.2%	8.8%	-3.6%	-3.3%	2.8%	-6.4%	1.9%	-9.4%	-2.3%	-5.7%	-2.5%	-6.5%

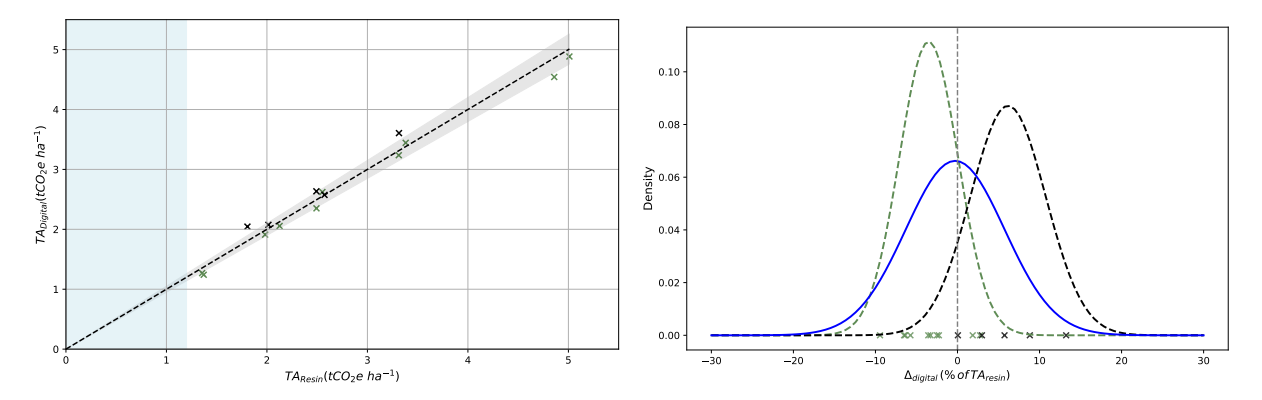


Figure 7: (Left) Comparison of digital TA signal $(TA_{digital})$ against chemically recovered alkalinity (TA_{resin}) . Green symbols denoting no-soil and black symbols soil devices respectively. The dashed line represents the 1:1 ideal relationship, the shaded band indicates a $\pm 5\%$ margin and the blue shaded region indicates the range used for sensor calibration. (Right) Distribution of digital deviation $\Delta_{digital}$ for soil (black), no-soil (green) and all units (blue), showing normal error distribution (no-soil mean = -3.5%, SD = 3.6%; soil mean = 6.2%, SD = 4.6%; overall mean = -0.3%, SD = 6.0%).

Overall Performance

Performance results are summarized in table 9. Across all 15 devices that received alkalinity, the Pulsar delivered consistently strong performance under both soil and no-soil conditions. Capture efficiencies were 98.9% without soil and at least 97.7% with soil, confirming that the weak acid resin system retains nearly all alkalinity entering the device across the full operational loading range. Back-titration recovered 98.8% (no soil) and at least 93.9% (soil), indicating that the chemical readout remains quantitative even under more complex soil chemistry and high loading states. Despite the small positive bias observed for the soil cohort, which we attribute to alkalinity retained within the soil column, the titration reliably reflects the alkalinity accumulated in the resin, with the true expected recovery efficiency

likely being closer to the observed capture efficiency.

Table 9: Summary of sensor performance across capture efficiency $\eta_{capture}$, combined capture & recovery efficiency $\eta_{recovery}$ and electronic sensor performance $\Delta_{digital}$.

Performance Metric	Type	Measurement	Accuracy error	Precision error
$\eta_{capture}$	No soil Soil	98.9% > 97.7%	$0.3\% \ 0.3\%$	$0.5\% \\ 0.5\%$
$\eta_{recovery}$	No soil	98.8%	0.2%	4.1%
	Soil	>93.9%	<4.0%	1.3%
$\Delta_{digital}$	No soil	-	-3.5%	3.6%
	Soil	-	6.2%	4.6%
	Total	-	-0.3 %	6.0%

Mass-balance residuals averaged 0.1% (SD=4.3) for sensors without soil and 4.0% (SD=1.3) for sensors with soil, consistent with expected analytical uncertainty. Digital measurements closely matched chemically recovered alkalinity with a mean deviation of -0.3% (SD=6.0%). Together, these results validate both the chemical and electronic subsystems of the Pulsar and demonstrate its ability to quantify cumulative alkalinity export with high accuracy under soil percolation conditions.

Conclusions

This study provides the first quantitative validation of the Pulsar, a field-deployable alkalinity sensor capable of directly measuring cumulative alkalinity export, under controlled soil-column conditions. Across 15 functional units receiving alkalinity over a 7-day continuous-flow experiment, the sensor achieved quantitative capture and recovery of TA (> 98% without soil; > 94% with soil) and low average TA-associated cation mass-balance residuals (0.1% without soil; 4.0% with soil). Effluent TA remained below 2 %, and digital signal deviation from titrated ground truth averaged just -0.3% (SD=6.0%), demonstrating high accuracy and solid precision of the electronic readout. While a small bias due to unmeasured desorp-

tion of cations in the soil remains, the difference to the no-soil cohort speaks for the retained alkalinity hypothesis. The complexity of full soil ion mass-balance measurements observed in this study further underscores the value of a direct net alkalinity export measurement for EW CDR.

These results confirm that weak-acid ion-exchange resins can serve as a quantitative measurement for alkalinity export in Enhanced Weathering settings and that the presented electronic transduction mechanism reliably quantifies cumulative TA uptake in real time. The combination of robust resin capture and digital quantification provides a scalable framework for real-time, in situ monitoring, reporting, and verification of EW carbon removal. Future work will focus on field-scale validation of the sensor's hydrological representativeness across soil textures and climatic regimes, and integration into long-term deployments.

By enabling continuous, automated measurement of alkalinity export directly in the field, the presented technology provides a breakthrough MRV tool for EW and establishes a practical foundation for rigorous, cost-effective, and scalable verification of carbon removal as the industry advances to larger deployments.

Appendix

Table 10: Measured sodium concentrations in the effluent as % of device specific input sodium concentrations. All times are CET. Note that dummy sensor values as % input are not reported here as they received DI water.

Device ID	Oct 14 7.35 pm	Oct 15 10.21 am	Oct 15 5.50 pm	Oct 16 9.37 am	Oct 16 10.19 pm	Oct 17 8.57 am	Oct 17 9.48 pm	Oct 18 10.14 am	Oct 19 12.48 pm	Oct 20 8.33 am	Oct 21 10.59 am
1	4.69	3.34	2.71	1.85	1.69	1.12	1.21	1.26	_	_	_
2	4.40	2.75	2.20	1.81	1.61	1.52	1.29	1.31	_	_	_
3	5.66	2.84	2.40	1.93	1.67	1.10	_	_	_	_	_
4	3.80	2.53	2.13	1.68	1.47	1.41	_	_	_	_	_
5	6.70	3.21	_	2.14	1.63	1.26	1.25	1.37	1.35	_	_
6	1.78	1.12	1.2	0.73	0.74	0.77	_	_	_	_	_
7	1.65	1.08	0.98	0.58	0.80	0.80	_	_	_	_	_
8	1.73	1.13	1.11	0.70	0.72	0.86	0.89	0.79	_	_	_
9	2.25	1.21	1.02	0.65	_	_	_	_	_	_	
10	1.84	1.21	0.99	0.67	0.75	0.73	0.76	0.73	0.71	_	_
11	1.88	1.08	1.03	0.83	_	_	_	_	_	_	_
12	2.10	0.99	1.07	0.81	0.73	0.77	0.84	0.76	0.58	_	_
13	2.01	1.23	0.68	0.82	0.80	0.64	0.81	0.80	_	_	_
14	1.68	1.24	1.13	0.83	0.90	0.75	0.89	0.77	0.75	0.88	1.99
15	1.93	1.12	1.04	0.76	0.62	0.75	0.84	0.72	0.65	0.89	1.58

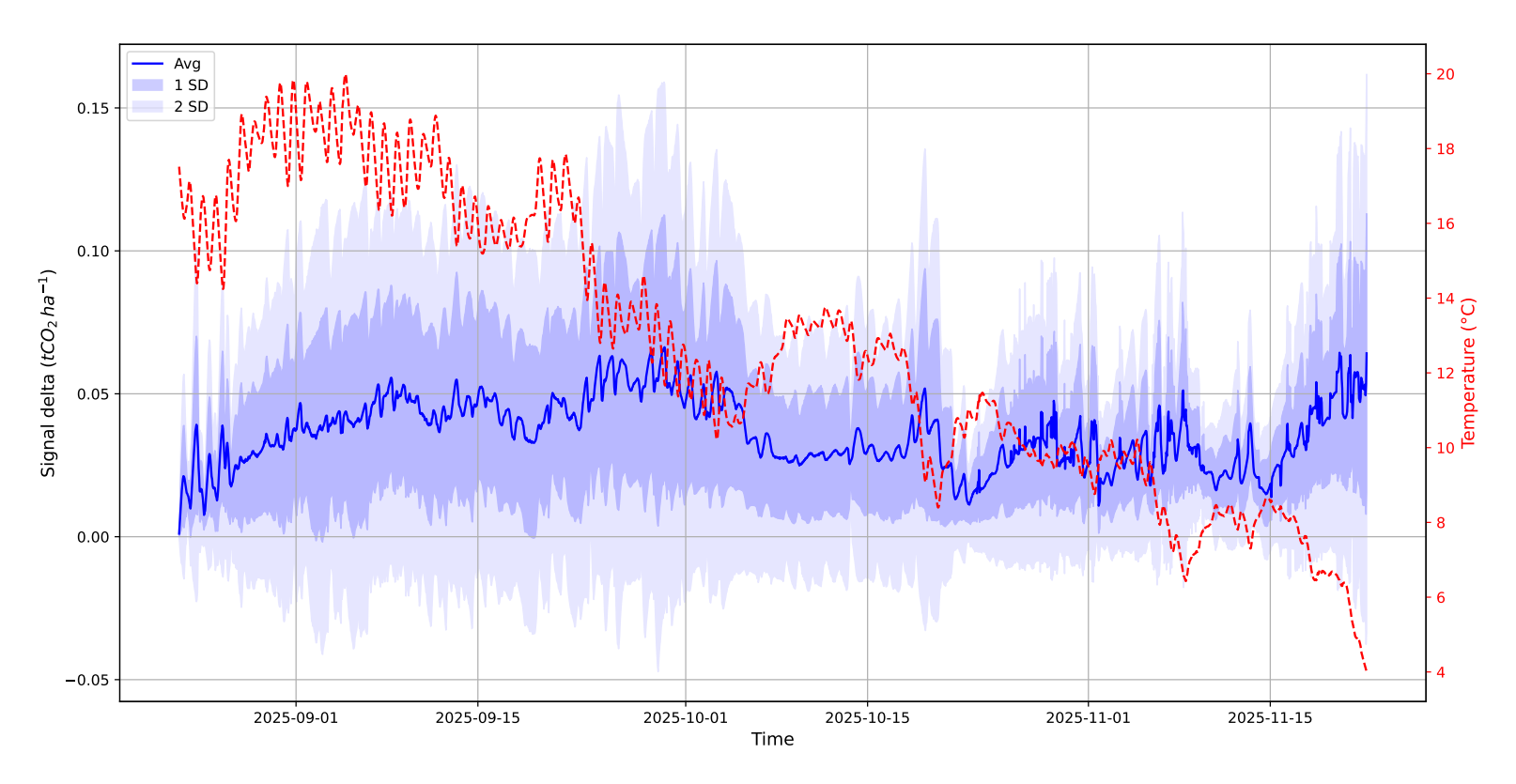


Figure 8: Digital TA signal data from a field deployment with six units (n = 6) evaluating environmental noise compensation using "dummy" sensors, which contain mixed-bed resin to adsorb all ions before percolation water reaches the weak-acid resin. The average signal difference between the two groups (blue; Group 1: n = 3, Group 2: n = 3) remains low and stable throughout daily temperature cycling and across a seasonal temperature decline of more than 15°C over three months, demonstrating effective suppression of environmental noise.

References

- (1) Beerling, D. J. et al. Potential for Large-Scale CO2 Removal via Enhanced Rock Weathering with Croplands. *Nature* **2020**, *583*, 242–248.
- (2) Fuhrman, J.; Bergero, C.; Weber, M.; Monteith, S.; Wang, F. M.; Clarens, A. F.; Doney, S. C.; Shobe, W.; McJeon, H. Diverse Carbon Dioxide Removal Approaches Could Reduce Impacts on the Energy-Water-Land System. *Nature Climate Change* 2023, 13, 341–350.
- (3) Beerling, D. J. et al. Transforming US Agriculture for Carbon Removal with Enhanced Weathering. *Nature* **2025**, *638*, 425–434.
- (4) Clarkson, M. O.; Larkin, C. S.; Swoboda, P.; Reershemius, T.; Suhrhoff, T. J.; Maesano, C. N.; Campbell, J. S. A Review of Measurement for Quantification of Carbon Dioxide Removal by Enhanced Weathering in Soil. Frontiers in Climate 2024, 6.
- (5) Almaraz, M.; Bingham, N. L.; Holzer, I. O.; Geoghegan, E. K.; Goertzen, H.; Sohng, J.; Houlton, B. Z. Methods for Determining the CO2 Removal Capacity of Enhanced Weathering in Agronomic Settings. Frontiers in Climate 2022, 4.
- (6) Suhrhoff, T. J.; Reershemius, T.; Wang, J.; Jordan, J. S.; Reinhard, C. T.; Planavsky, N. J. A Tool for Assessing the Sensitivity of Soil-Based Approaches for Quantifying Enhanced Weathering: A US Case Study. Frontiers in Climate 2024, 6.
- (7) Reershemius, T.; Kelland, M. E.; Jordan, J. S.; Davis, I. R.; D'Ascanio, R.; Kalderon-Asael, B.; Asael, D.; Suhrhoff, T. J.; Epihov, D. Z.; Beerling, D. J.; Reinhard, C. T.; Planavsky, N. J. Initial Validation of a Soil-Based Mass-Balance Approach for Empirical Monitoring of Enhanced Rock Weathering Rates. *Environmental Science & Technology* 2023,

- (8) Kanzaki, Y.; Planavsky, N. J.; Zhang, S.; Jordan, J.; Suhrhoff, T. J.; Reinhard, C. T. Soil Cation Storage Is a Key Control on the Carbon Removal Dynamics of Enhanced Weathering. *Environmental Research Letters* 2025, 20, 074055.
- (9) Foundations for Carbon Dioxide Removal Quantification in ERW Deployments. https://cascadeclimate.org/blog/foundations-for-carbon-removal-quantification-in-erw-deployments.
- (10) Hartmann, J.; West, A. J.; Renforth, P.; Köhler, P.; Rocha, C. L. D. L.; Wolf-Gladrow, D. A.; Dürr, H. H.; Scheffran, J. Enhanced Chemical Weathering as a Geoengineering Strategy to Reduce Atmospheric Carbon Dioxide, Supply Nutrients, and Mitigate Ocean Acidification.
- (11) Beerling, D. J. et al. Enhanced Weathering in the US Corn Belt Delivers Carbon Removal with Agronomic Benefits. Proceedings of the National Academy of Sciences 2024, 121, e2319436121.
- (12) Beerling, D. J. et al. Farming with Crops and Rocks to Address Global Climate, Food and Soil Security. *Nature Plants* **2018**, *4*, 138–147.
- (13) McBride, A. L. et al. Quantifying Potential Carbon Dioxide Removal via Enhanced Weathering Using Porewater from a Field Trial in Scotland. Frontiers in Climate 2025, 7.
- (14) Power, I. M.; Hatten, V. N. J.; Guo, M.; Schaffer, Z. R.; Rausis, K.; Klyn-Hesselink, H. Are Enhanced Rock Weathering Rates Overestimated? A Few Geochemical and Mineralogical Pitfalls. *Frontiers in Climate* **2025**, 6.
- (15) Fernando, S. U.; Galagedara, L.; Krishnapillai, M.; Cuss, C. W. Lysimeter Sampling System for Optimal Determination of Trace Elements in Soil Solutions. *Water* **2023**, 15, 3277.

- (16) Lehmann, J.; Kaiser, K.; Peter, I. Exchange Resin Cores for the Estimation of Nutrient Fluxes in Highly Permeable Tropical Soil. *Journal of Plant Nutrition and Soil Science* **2001**, *164*, 57–64.
- (17) Lang, F.; Kaupenjohann, M. Trace Element Release from Forest Floor Can Be Monitored by Ion Exchange Resin Tubes. *Journal of Plant Nutrition and Soil Science* 2004, 167, 177–183.
- (18) Johnson, D. W.; Verburg, P. S. J.; Arnone, J. A. Soil Extraction, Ion Exchange Resin, and Ion Exchange Membrane Measures of Soil Mineral Nitrogen During Incubation of a Tallgrass Prairie Soil. Soil Science Society of America Journal 2005, 69, 260–265.
- (19) Predotova, M.; Bischoff, W.-A.; Buerkert, A. Mineral-Nitrogen and Phosphorus Leaching from Vegetable Gardens in Niamey, Niger. Zeitschrift für Pflanzenernährung und Bodenkunde 2011, 174, 47–55.
- (20) Grahmann, K.; Verhulst, N.; Palomino, L. M.; Bischoff, W.-A.; Govaerts, B.; Buerkert, A. Ion Exchange Resin Samplers to Estimate Nitrate Leaching from a Furrow Irrigated Wheat-Maize Cropping System under Different Tillage-Straw Systems. Soil and Tillage Research 2018, 175, 91–100.
- (21) Kunin, R.; Vassiliou, B. New Deionization Techniques Based upon Weak Electrolyte Ion Exchange Resins. *Industrial & Engineering Chemistry Process Design and Development* **1964**, *3*, 404–409.
- (22) Dragull, K.; Beck, J. J. Isolation of Natural Products by Ion-Exchange Methods. *Methods in Molecular Biology (Clifton, N.J.)* **2012**, *864*, 189–219.
- (23) Gupta, S.; Hengl, T.; Lehmann, P.; Bonetti, S.; Or, D. SoilKsatDB: Global Database of Soil Saturated Hydraulic Conductivity Measurements for Geoscience Applications. Earth System Science Data 2021, 13, 1593–1612.